LEVEL II

DNA 5593T

AD A105824

GLASS FRAGMENT HAZARD FROM WINDOWS BROKEN BY AIRBLAST

E. Royce Fletcher
Donald R. Richmond
John T. Yelverton
Lovelace Biomedical and Environmental
Research Institute,Inc
P.O. Box 5890
Albuquerque, New Mexico 87185

DTIC
ELECTE
OCT 1 9 1981
H

30 May 1980

Topical Report for Period 30 May 1979—30 May 1980

CONTRACT No. DNA IACRO-76-634

APPROVED FOR PUBLIC RELEASE;
DISTRIBUTION UNLIMITED.

THIS WORK SPONSORED BY THE DEFENSE NUCLEAR AGENCY
UNDER RDT&E RMSS CODE B350076464 U99QAXMA01204 H2590D.

DTIC FILE COPY

Prepared for
Director
DEFENSE NUCLEAR AGENCY
Washington, D. C. 20305

1 0 19

Destroy this report when it is no longer needed. Do not return to sender.

PLEASE NOTIFY THE DEFENSE NUCLEAR AGENCY, ATTN: STTI, WASHINGTON, D.C. 20305, IF YOUR ADDRESS IS INCORRECT, IF YOU WISH TO BE DELETED FROM THE DISTRIBUTION LIST, OR IF THE ADDRESSEE IS NO LONGER EMPLOYED BY YOUR ORGANIZATION.

UNCLASSIFIED

SECURITY CLASSIFICATION OF THIS PAGE (When Data Entered)

REPORT DOCUMENTATION PAGE

READ INSTRUCTIONS BEFORE COMPLETING FORM

1. REPORT NUMBER: DNA 5593T	2. GOVT ACCESSION NO.: AD-A105824
3. RECIPIENT'S CATALOG NUMBER:	
4. TITLE (and Subtitle): GLASS FRAGMENT HAZARD FROM WINDOWS BROKEN BY AIRBLAST	5. TYPE OF REPORT & PERIOD COVERED: Topical Report for Period 30 May 79 — 30 May 80
	6. PERFORMING ORG. REPORT NUMBER:
7. AUTHOR(s): E. Royce Fletcher, Donald R. Richmond, John T. Yelverton	8. CONTRACT OR GRANT NUMBER(s): DNA-IACRO-76-634, DE-AC04-76-EV01013
9. PERFORMING ORGANIZATION NAME AND ADDRESS: Lovelace Biomedical and Environmental Research Institute, Inc. P. O. Box 5890 Albuquerque, New Mexico 87185	10. PROGRAM ELEMENT, PROJECT, TASK AREA & WORK UNIT NUMBERS: Subtask U99QAXMA012-04
11. CONTROLLING OFFICE NAME AND ADDRESS: Director, Defense Nuclear Agency, Washington, D. C. 20305	12. REPORT DATE: 30 May 1980
	13. NUMBER OF PAGES: 42
14. MONITORING AGENCY NAME & ADDRESS (if different from Controlling Office)	15. SECURITY CLASS (of this report): UNCLASSIFIED
	15a. DECLASSIFICATION DOWNGRADING SCHEDULE: N/A

16. DISTRIBUTION STATEMENT (of this Report)

Approved for public release; distribution unlimited.

17. DISTRIBUTION STATEMENT (of the abstract entered in Block 20, if different from Report)

18. SUPPLEMENTARY NOTES

This work sponsored by the Defense Nuclear Agency under RDT&E RMSS Code B350076464 U99QAXMA01204 H2590D.

19. KEY WORDS (Continue on reverse side if necessary and identify by block number)

Glass fragment injuries
Window glass missiles
Glass fragment parameters
Biophysics of glass fragments
Penetrating wounds
Shatter overpressure of windows
Airblast on windows

20. ABSTRACT (Continue on reverse side if necessary and identify by block number)

This report presents shatter overpressures as a function of window size and orientation. Average values for fragment velocity, mass, and spatial density are given in relation to blast overpressure. The velocities of fragments for 50-percent probability of skin and body-wall penetration in addition to skull fracture are presented as functions of fragment mass. The protection afforded by clothing is indicated. The number of wounds and their severity is predicted as a function of either fragment velocity or blast overpressure for people behind windows in structures.

DD FORM 1 JAN 73 1473 EDITION OF 1 NOV 65 IS OBSOLETE

UNCLASSIFIED

SECURITY CLASSIFICATION OF THIS PAGE (When Data Entered)

393521

CONVERSION FACTORS FOR METRIC (SI) TO U.S. CUSTOMARY
UNITS OF MEASUREMENT

Multiply	By	To Obtain
millimeters	0.03937008	inches
centimeters	0.3937008	inches
square centimeters	0.1550003	square inches
meters	3.280840	feet
square meters	10.76391	square feet
kilometers	0.6213712	miles
meters per second	3.280840	feet per second
fragments per square meter	0.09290304	fragments per square foot
grams	0.002204622	pounds-mass
grams per square meter	0.02949352	ounces per square yard
grams per cubic centimeter	62.42796	pounds-mass per cubic foot
kilopascals	0.1450377	pounds-force per square inch (psi)

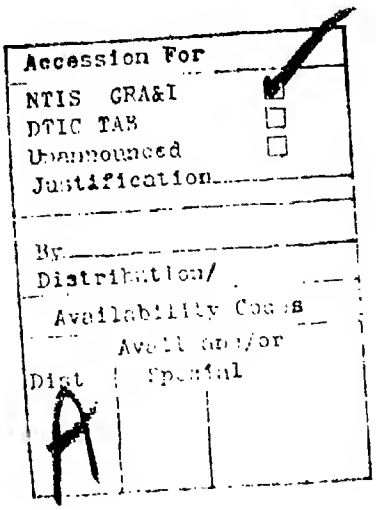

PREFACE

This research was supported by the Defense Nuclear Agency via Contract No. IACRO-76-834 under U. S. Department of Energy Contract No. DE-AC04-76-EV01013.

This study was under the direction of R. K. Jones. The technical assistance of K. Saunders, W. Hicks, R. Clark, and A. Shaw is acknowledged. T. Minagawa performed the technical photography and prepared the illustrative material. B. Martinez provided editorial assistance and processed the final manuscript.

This research was conducted according to the principles enunciated in the "Guide for Laboratory Animal Facilities and Care," prepared by the National Academy of Sciences, National Research Council.

PRECEDING PAGE BLANK-NOT FILMED

TABLE OF CONTENTS

Section		Page
	PREFACE	3
	LIST OF ILLUSTRATIONS	4
	LIST OF TABLES	6
I	INTRODUCTION	7
	A. Objectives	7
	B. Background	7
II	NATURE OF WINDOW BREAKUP	8
III	OVERPRESSURE TO SHATTER WINDOWS	11
IV	FRAGMENT VELOCITY AND MASS	11
V	SPATIAL DENSITY OF FRAGMENTS	20
VI	BIOLOGICAL EFFECTS	22
	A. Individual Fragments	22
	B. Windows	30
VII	PREDICTION OF WOUNDS VS OVERPRESSURE	32
	REFERENCES	35

LIST OF ILLUSTRATIONS

Figure		Page
1	Reconstructions of three 30x48x0.17-cm panes of sheet glass broken by a sonic boom with a peak incident overpressure of about 3 kPa (after reference 4)	9
2	Postshot view of the interior of a room in which two 122x229x0.607-cm panes of glass were exposed face-on to a large HE detonation at an incident overpressure of 4 kPa (after reference 3)	10
3	Free-field incident overpressure for 50-percent probability of failure of a window oriented face-on to a blast wave (after reference 2)	12
4	Peak blast-wave overpressure on a window for 50-percent probability of failure (after reference 2)	13

LIST OF ILLUSTRATIONS (continued)

Figure		Page
5	Velocities and masses of fragments trapped in a witness plate 2.1 m behind two 107x51x0.317-cm glass panes exposed face-on to a large HE detonation at an incident overpressure of 4 kPa (after reference 3)	14
6	Scaled geometric-mean fragment velocity vs peak overpressure on the window (after reference 3)	15
7	Glass-fragment velocities for a window mounted in a house or on the end-plate closing a shock tube vs peak overpressure on the window	18
8	Geometric-mean frontal area of fragments vs peak overpressure on the window (after reference 3)	19
9	Scaled average maximum density of trapped fragments plus 22.28 vs peak overpressure on the window (after reference 3)	21
10	(Average density of fragments trapped at an angle of ψ)/(average maximum density of trapped fragments) vs angle, ψ, beyond the edge of the window	21
11	Fifty-percent probability of fragments penetrating skin on the thorax or abdomen	26
12	Fifty-percent probability of fragments penetrating body wall of the thorax or abdomen	27
13	Fifty-percent probability of fragments penetrating skin on the head	28
14	Fifty-percent probability of fragments fracturing the skull	28
15	Effects of clothing on fragment velocities required to penetrate skin or body wall	29
16	Glass-fragment injuries to subjects behind windows exposed to airblast vs mean impact velocity of the fragments	31
17	Glass-fragment injuries to subjects behind windows exposed to airblast vs effective peak overpressure on the window	34

LIST OF TABLES

Table		Page
1	Injuries to sheep behind glass windows mounted on the end-plate closing a shock tube	16
2	Fragment velocities for 50-percent probability of indicated injuries to sheep or dogs	23

I. INTRODUCTION

A. Objectives

The objectives of this study were:

1. to review the available information on the velocities, masses, and spatial distributions of glass fragments from windows broken by airblast;

2. to summarize the results from experiments to assess the biological effects of window fragments; and

3. to predict the glass-fragment hazards inside structures in relation to blast overpressure.

B. Background

For the nuclear detonations in Japan, the most far-reaching blast hazard to people inside structures was from window-glass fragments. Patients were treated for lacerations received out to 3.2 km from ground zero in Hiroshima and out to 3.8 km in Nagasaki (Reference 1). In both cities, the area of glass breakage was nearly sixteen times as great as the area of significant structural damage.

Laboratory studies have provided information on the overpressure levels required to shatter windows (Reference 2). Velocities, masses, and spatial distributions of fragments have been measured by trapping the fragments in Styrofoam® (expanded polystyrene) witness plates located behind windows in houses subjected to large chemical or nuclear explosions (References 3 and 4). Yields ranged from 14 tons HE to 29 KT nuclear and incident overpressures ranged from 2 to 34 kPa.

Biological effects have been studied using individual glass fragments fired from an airgun and impacted against anesthetized dogs and sheep (Reference 5). A similar study was conducted with acrylic fragments (cited in Reference 4). Anesthetized sheep have been exposed behind glass windows mounted on the end of a shocktube, and dogs have been exposed behind windows in a house subjected to a nuclear detonation (Reference 6).

II. NATURE OF WINDOW BREAKUP

When a glass pane is dislodged from its mounting by a blast wave, normally almost the entire exposed, or unclamped, portion of the pane shatters into numerous fragments whose size generally decreases with increasing overpressure. Figure 1 shows reconstructions of three typical window panes broken by a sonic boom with a peak incident overpressure of approximately 3 kPa. Most of the fragments had one or more sharp points, but there was a wide variety of shapes. In general, the cleavage surfaces were approximately perpendicular to the planar surfaces of the fragments.

Motion-picture records have shown the breakage of glass windows with either two 91x91x0.305-cm panes or one 137x183x0.574-cm pane mounted on the end-plate closing a shock-tube. For either type of window, the fragments appeared to form a cloud which expanded in all directions as it translated. Most of the fragments underwent significant rotation before they had translated 2 m. However, many of the fragments could not be characterized as tumbling and in a random orientation. The leading half of a cloud was roughly hemispherical in shape with a significant number of the larger fragments appearing to have their flat surfaces tangent to the hemisphere. This tendency was diminished, but still evident, at 4 m. The fragments in the trailing half of a cloud appeared to be randomly oriented before they had translated 2 m. In general, for a given overpressure, the larger panes produced larger fragments which tumbled less than the fragments from the smaller panes.

Figure 2 is a post-shot view of the interior of a room in which two 122x229x0.607-cm panes of glass were exposed face-on to a shockwave having a peak incident overpressure of 4 kPa (Reference 3). Forty-six fragments were trapped in the witness plate located 2.1 m downstream of the window. Other, persumably less hazardous, fragments struck the Styrofoam® leaving impressions but were not retained. Still other fragments missed the witness plate entirely. Many fragments can be seen either laying on the floor or still retained in the frame.

PANE NO. 1

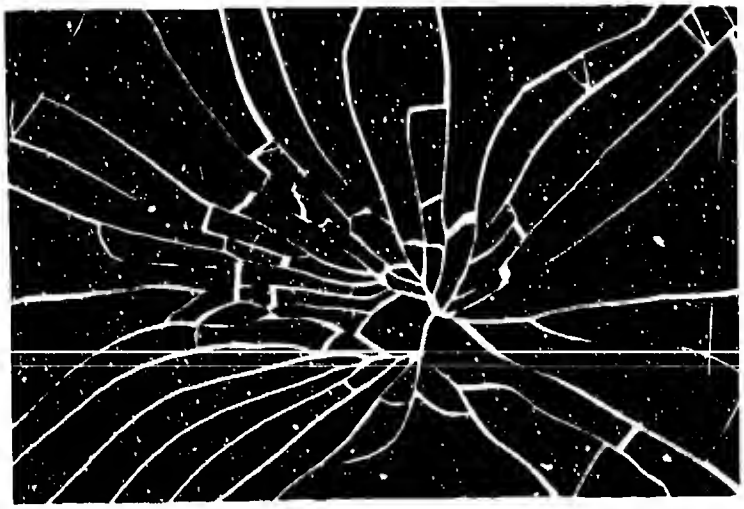

PANE NO. 2

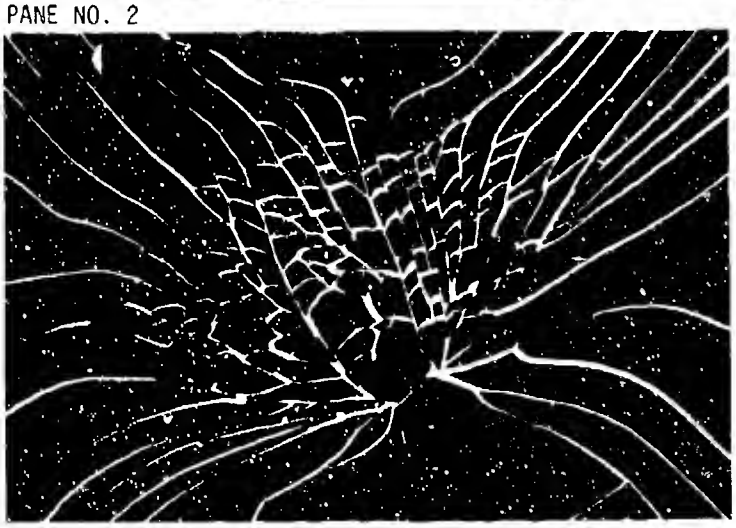

PANE NO. 3

Figure 1. Reconstructions of three 30x48x0.17-cm panes of sheet glass broken by a sonic boom with a peak incident overpressure of about 3 kPa (after reference 4).

Figure 2. Postshot view of the interior of a room in which two 122x229x0.607-cm panes of glass were exposed face-on to a large HE detonation at an incident overpressure of 4 kPa (after reference 3).

III. OVERPRESSURE TO SHATTER WINDOWS

The peak overpressure required to shatter a window in a building has been found to be a function of pane area and thickness, type of glass and mounting used, orientation of the window with respect to the blast wave, flaws in the glass, and stresses introduced when the pane was mounted. Figures 3 and 4 show predictions for a 50-percent probability of failure of sheet- and plate-glass windows oriented either face- or side-on to the blast wave (Reference 2) Each line in the figures extends across the range of pane areas normally used for glass of the indicated type and thickness. These predictions were derived for an explosive yield greater than 1 KT, a clearing distance (i.e., the distance from the center to the edge of the wall containing the face-on window) greater than 6 m, and an aspect ratio of the pane greater than 1/3. It was recommended that thin, weak muntins be ignored, and thus the area within substantial frame members be considered as the pane area.

In Figure 3, it can be seen that the incident overpressure for a 50-percent probability of failure is between 0.6 and 6.0 kPa for most face-on windows. Note also that the type of glass, plate or sheet, influences the overpressure required for failure more for thin panes than it does for thick panes. For a small, thin pane exposed to a relatively high overpressure, the failure time could be short compared to the time required for a rarefraction wave to travel the clearing distance. In such cases, the probability of breakage should be influenced more by the peak overpressure on the window than by its orientation. Figure 4 shows that, for a 50-percent failure rate of ordinary single- or double-strength sheet-glass windows, the peak overpressure on the window is essentially the same for the face- and side-on orientations.

IV. FRAGMENT VELOCITY AND MASS

Figure 5 gives the velocities and masses of the 87 fragments trapped 2.1 m behind a glass window with two 107x51x0.317-cm panes oriented face-on in a room exposed to a 175-ton HE detonation at a peak incident overpressure of 4 kPa (Reference 3). Only the data for trapped fragments are plotted because the velocity and mass of a fragment that was not retained in the witness plate could be estimated only in those cases where the impression was

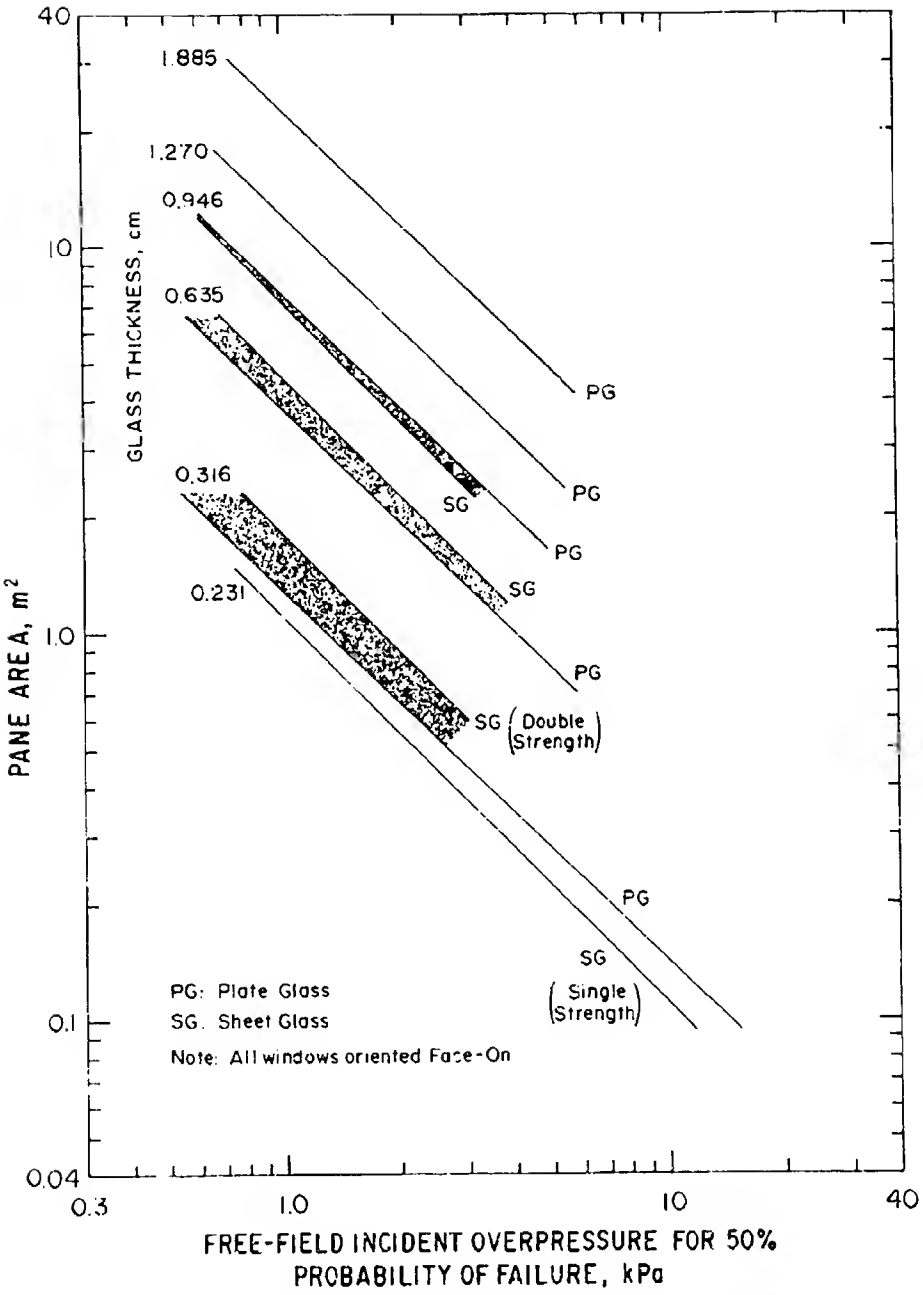

Figure 3. Free-field incident overpressure for 50-percent probability of failure of a window oriented face-on to a blast wave (after reference 2).

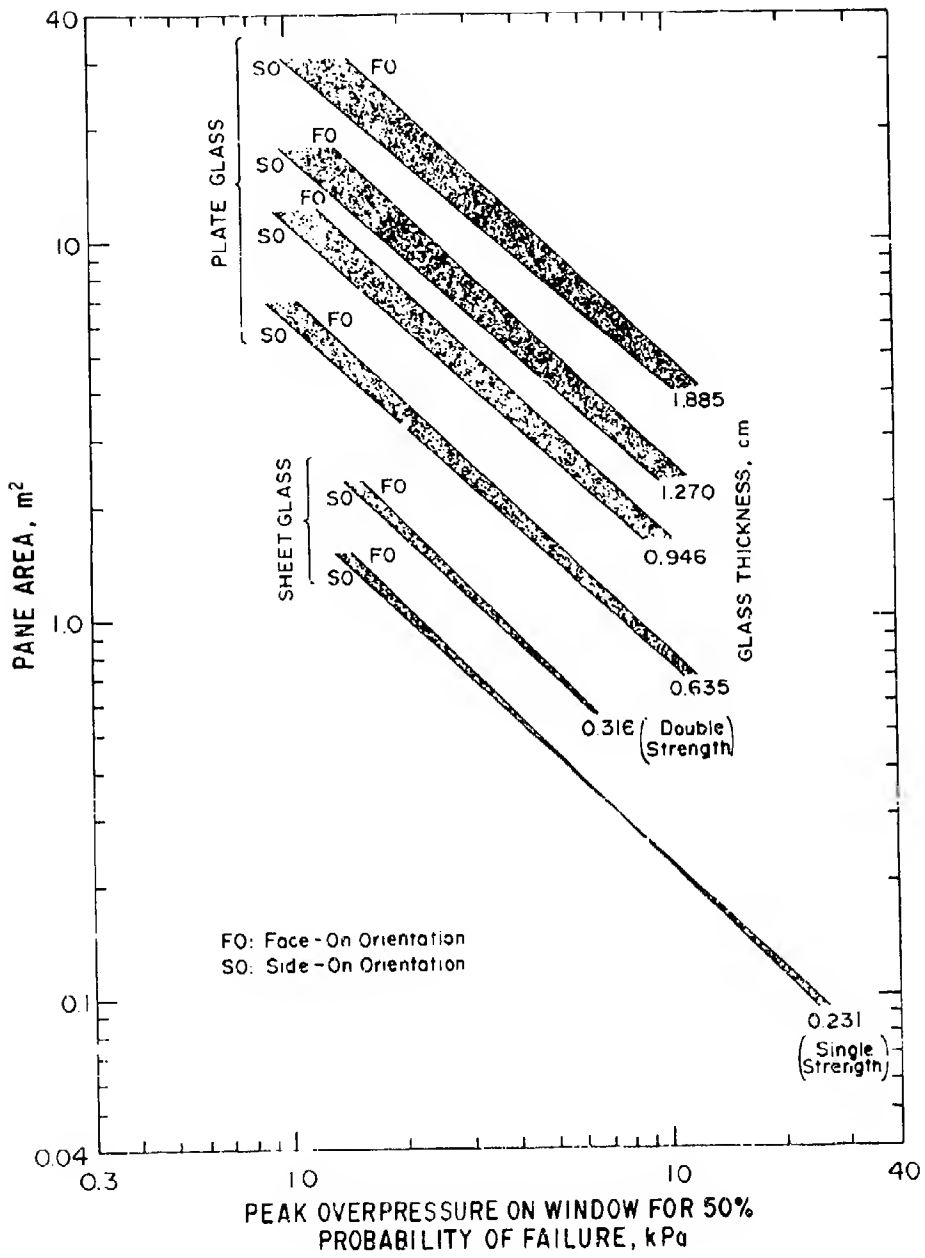

Figure 4. Peak blast-wave overpressure on a window for 50-percent probability of failure (after reference 2).

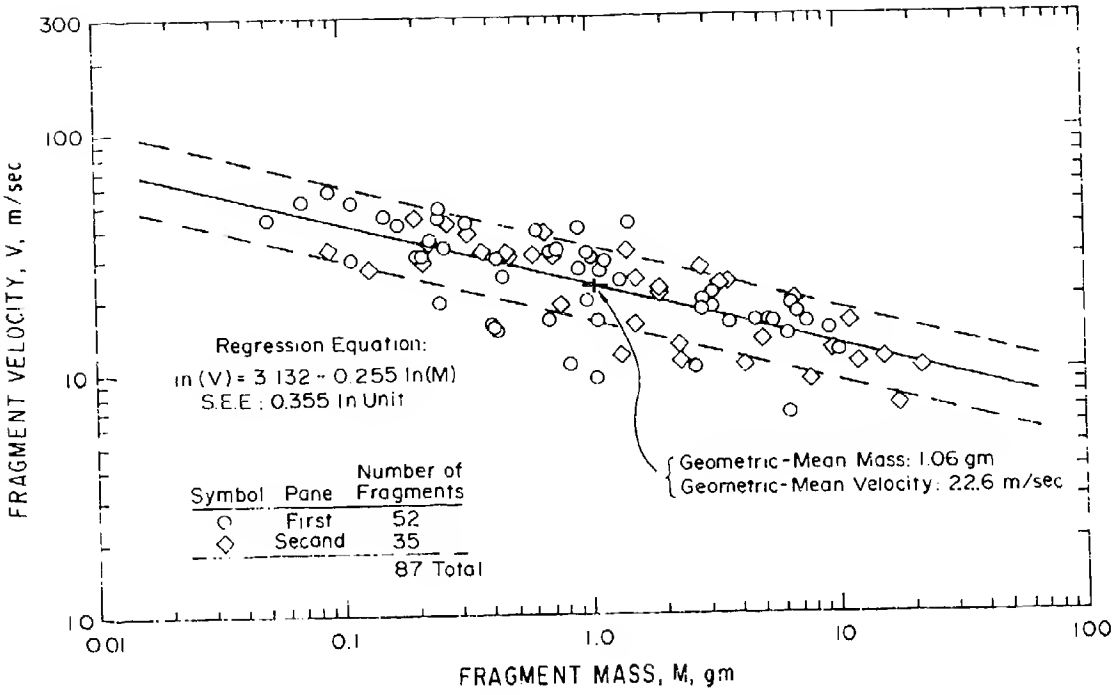

Figure 5. Velocities and masses of fragments trapped in a witness plate 2.1 m behind two 107x51x0.317-cm glass panes exposed face-on to a large HE detonation at an incident overpressure of 4 kPa (after reference 3).

relatively flat. Neither the velocities, ranging from 7 to 56 m/sec, nor the masses, ranging from 0.05 to 22 gm, showed a significant variation with impact location. The results of a least-squares linear-regression analysis appear as a solid line, and dashed lines are drawn one standard error of estimate above and below the regression line. The geometric-mean velocity and mass are indicated by a "+" on the regression line.

Figure 6 is a plot of geometric-mean fragment velocity vs peak overpressure on 0.3175-cm-thick glass windows in 1- and 2-story houses exposed to a long-duration blast wave (Reference 3). The data were obtained using explosive yields varying from 14 tons HE to 29 KT nuclear, distances between windows and witness plates ranging from 0.9 to 5.2 m, and pane thicknesses between 0.163 and 0.671 cm. A scaling factor, given in the figure, was used to adjust the velocities for glass thicknesses other than 0.3175 cm.

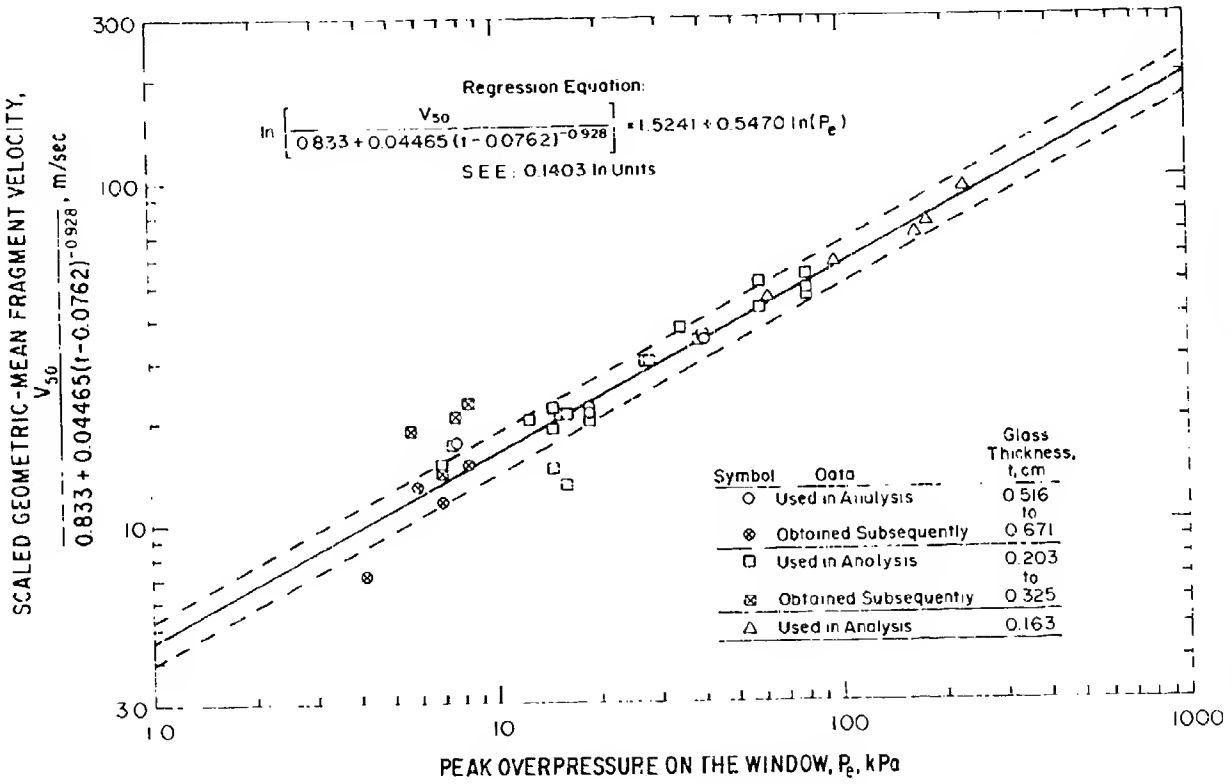

Figure 6. Scaled geometric-mean fragment velocity vs peak overpressure on the window (after reference 3).

This factor indicates that the geometric-mean velocity was 14 percent greater for 0.203-cm glass, and 9 percent less for 0.671-cm glass, than the corresponding velocity for 0.1375-cm glass. Although the overpressure required to break a window was approximately inversely proportional to pane area (Figure 4), the geometric-mean fragment velocity (Figure 6) seemed to be reasonably independent of pane area.

Velocities were also measured from the motion-picture records showing the clouds of fragments emanating from glass windows mounted on the end-plate closing a shocktube (Table 1). The maximum velocities of both the leading edge and the middle of each cloud, in addition to the time (measured from when the blast wave first struck the window) and translation distance required for the leading edge to reach maximum velocity, were determined. As the incident overpressure increased, the acceleration times decreased, and the

TABLE 1

INJURIES TO SHEEP BEHIND GLASS WINDOWS MOUNTED ON THE END-PLATE CLOSING A SHOCKTUBE

Test No.	Peak Incident Overpressure, kPa	Peak Reflected Overpressure, kPa	Duration of Positive Phase of Overpressure, msec	Leading Edge of Fragment Cloud			Middle of Fragment Cloud Maximum Velocity, m/sec	Exposure Condition of Sheep	Number of			Maximum Wound Depth, cm	Percent of Exposed Surface Area† Sustaining	
				Acceleration Time, msec	Acceleration Distance, m	Maximum Velocity, m/sec			Incised Wounds	Skin Penetrations	Body-Wall Penetrations		Multiple Serious Wounds‡	Denudation
1	-	4	-	67	0.6	12	11	Bare Clothed	4 0	2 0	0 0	0.7 0.0	0 0	0 0
2	2	4	50	52	0.5	13	13	Bare Clothed	3 *	1 *	0 *	0.5 *	0 *	0 *
3	3	6	50	48	0.6	18	16	Bare Bare	37 36	10 9	0 0	1.2 1.4	0 0	0 0
4	3	7	60	49	0.7	23	21	Bare Bare	32 19	8 3	0 0	2.3 0.9	0 0	0 0
5	3	7	51	56	0.8	21	20	Clothed Clothed	6 8	0 1	0 0	0.2 1.0	0 0	0 0
6	3	7	50	47	0.7	23	22	Bare Bare	41 44	6 8	1 0	1.0 0.9	0 0	0 0
7	7	14	60	35	0.9	37	34	Bare Bare	73 57	6 6	0 0	1.0 1.2	0 0	0 0
8	7	14	68	38	0.9	34	31	Bare Bare	30 23	18 14	2 0	5.0 1.8	0.5 0	0 0
9	7	15	58	36	0.9	39	35	Clothed Clothed	5 21	: 6	0 0	0.6 1.3	0 0	0 0
10	13	28	100	25	1.0	64	53	Bare Clothed	236 39	84 8	6 2	3.4 4.0	3 0	0 0
11	14	29	86	26	0.9	59	52	Bare Bare	147 185	63 88	8 15	8.0 5.0	8 0	0 0
12	28	63	100	18	0.8	80	76	Bare Bare	127 282	87 79	5 8	5.0 6.9	12 24	6 15
13	2	5	53	47	0.2	10	9	Bare Clothed	14 5	0 1	0 0	0.4 0.4	0 0	0 0
14	2	5	52	45	0.3	10	9	Bare Clothed	6 1	3 0	0 0	0.9 0.2	0 0	0 0
15	3	8	47	44	0.3	16	14	Bare Clothed	38 3	15 0	0 0	1.1 0.2	0 0	0 0
16	4	8	50	33	0.3	17	16	Bare Clothed	49 10	22 4	0 0	1.7 1.4	0 0	0 0

See footnotes at end of table.

TABLE 1 (Continued)

INJURIES TO SHEEP BEHIND GLASS WINDOWS MOUNTED ON THE END-PLATE CLOSING A SHOCKTUBE

Test No.	Peak Incident Overpressure, kPa	Peak Reflected Overpressure, kPa	Duration of Positive Phase of Overpressure, msec	Leading Edge of Fragment Cloud			Middle of Fragment Cloud Maximum Velocity, m/sec	Exposure Condition of Sheep	Number of			Maximum Wound Depth, cm	Percent of Exposed Surface Area† Sustaining	
				Acceleration Time, msec	Acceleration Distance, m	Maximum Velocity, m/sec			Incised Wounds	Skin Penetrations	Body-Wall Penetrations		Multiple Serious Wounds#	Denudation
17	7	14	48	31	0.6	30	25	Bare Clothed	86 8	17 4	0 0	2.1 1.0	0 0	0 0
18	8	16	50	33	0.6	29	25	Bare Clothed	69 4	18 3	0 0	1.5 2.0	0 0	0 0
19	14	29	64	31	0.8	47	41	Bare Clothed	125 9	34 4	0 0	3.7 0.4	7 0	0 0
20	14	31	65	35	1.0	45	42	Bare Clothed	164 5	48 4	0 0	5.4 1.9	5 0	0 0
21	21	48	67	33	1.2	55	55	Bare Clothed	112 10	57 8	6 0	5.0 2.0	12 0	4 0
22	30	70	111	30	1.2	70	61	Bare Clothed	30 7	20 7	1 0	7.4 1.5	21 0	18 0
23	8	15	46	40	0.6	29	26	Bare Clothed	21 4	11 0	0 0	1.6 0.1	0 0	0 0
24	14	29	56	45	1.3	47	43	Bare Clothed	38 31	8 7	1 0	12.2 2.4	4 0	0 0
25	15	31	55	45	1.4	52	48	Bare Clothed	103 10	28 7	0 0	5.8 2.3	8 0	0 0

- Quantity could not be measured on gauge record.

* Window did not break.

† The exposed surface area was taken to be one-half of the total surface area of the sheep.

That is, one or more areas on the sheep had closely-clustered or contiguous wounds of greater than skin depth. Areas of denudation were also counted as areas of multiple, serious wounds.

Notes: The window consisted of two 91x91x0.305-cm panes for Tests 1-12 and one 137x183x0.574-cm pane for Tests 13-25.

The initial distance from glass to sheep was 2.1 m for Tests 1-22 and 4.3 m for Tests 23-25.

acceleration distances appeared to approach an upper limit of approximately 0.9 m for the 91x91-cm panes and 1.3 m for the 137x183-cm panes. In no case did the fragments appear to slow down significantly before reaching the biological targets at a distance of 2.1 or 4.3 m.

Independent of the overpressure level or type of window used, the maximum velocity of the leading edge of the cloud tended to be a factor of 1.10 times the maximum velocity of the middle of the cloud. For each shocktube test, the average impact velocity was taken to be the geometric mean of the maximum velocity of the middle of the cloud and the maximum velocity of the leading edge of the cloud divided by 1.10. These computed average velocities are plotted in Figure 7 as a function of the peak overpressure (i.e., the reflected overpressure) on the window. It can be seen that, for a given peak overpressure on the window, the mean fragment velocities for windows on the shocktube were greater

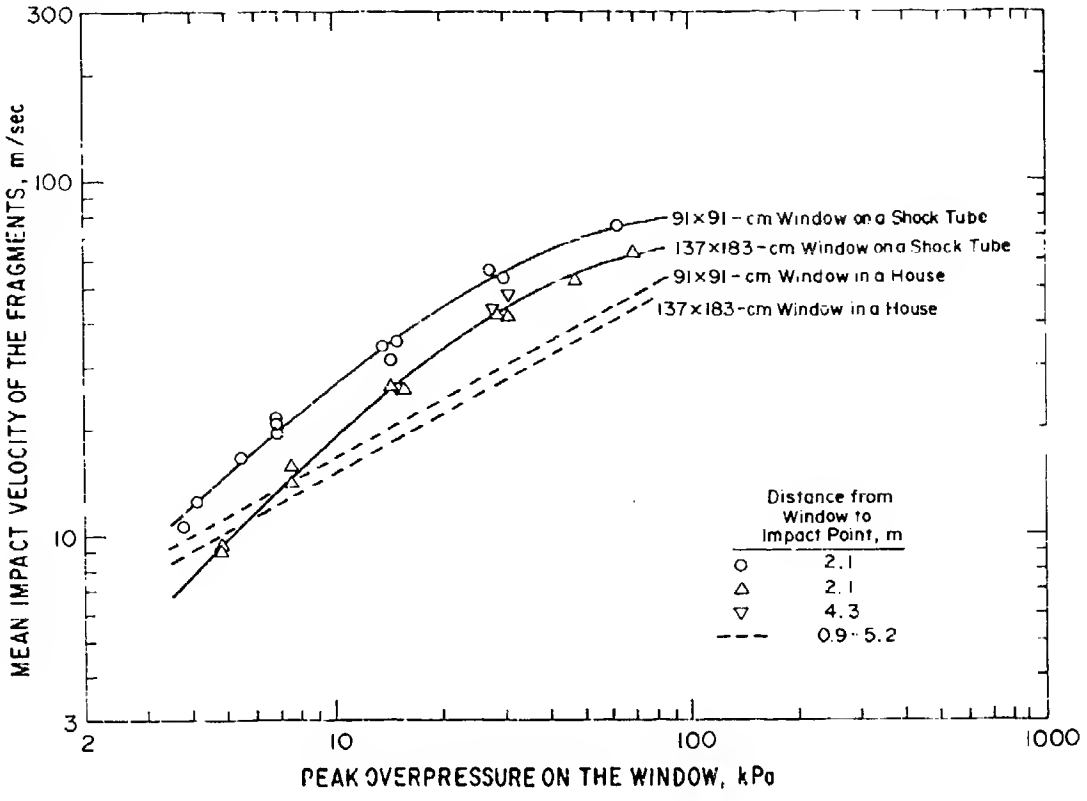

Figure 7. Glass-fragment velocities for a window mounted in a house or on the end-plate closing a shock tube vs peak overpressure on the window.

than the predictions (dashed lines), derived from the equation in Figure 6, for windows in houses. At least part of this difference was probably due to the fact that, for a house, the reflected pressure on a front-facing window decays to the stagnation pressure as the rarefaction wave coming from the edges of the front wall reaches the window, a condition that would not apply to windows mounted on the closed end of a shocktube.

Figure 8 is a plot of geometric-mean frontal area of trapped fragments vs peak overpressure on windows in 1- and 2-story houses (Reference 3). Each geometric-mean frontal area was computed by dividing the geometric-mean mass by both the pane thickness and the density of the glass used (2.47 gm/cm^3). The solid curve is the result of a least-

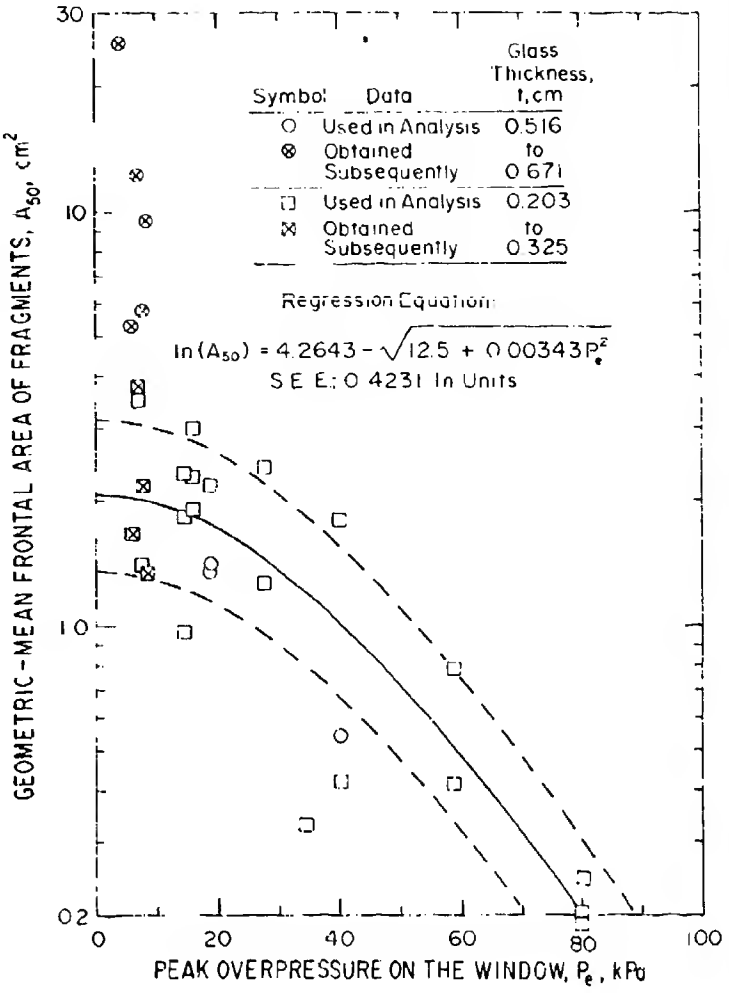

Figure 8. Geometric-mean frontal area of fragments vs peak overpressure on the window (after reference 3).

squares regression analysis and the dashed curves are drawn one standard error of estimate on either side. It can be seen that the geometric-mean frontal area decreases with increasing overpressure, and that the scatter in the mean areas is considerably larger than the scatter in the mean velocities (Figure 6). It should be noted that, at overpressures below 10 kPa, the measured frontal areas for thick glass (0.516 to 0.671 cm) were all larger than what would have been predicted using the regression equation.

V. SPATIAL DENSITY OF FRAGMENTS

For each window tested face-on in a house, the spatial density of fragments tended to be uniform over a portion of the witness plate equal in area to the window, but the density normally decreased beyond that area. This region of maximum density was directly behind the window except in instances where the fragment velocities were low and the witness plate was far from the window. In such cases, the maximum-density region was displaced downward due to gravity's acting on the fragments while they traversed the distance to the witness plate. Figure 9 is a plot of average density over the maximum density region plus 22.28 fragments/m^2 vs peak overpressure on 0.3175-cm-thick glass windows in houses exposed to a long-duration blast wave (Reference 3). The regression line predicts a density of 10 fragments/m^2 for an overpressure of 6.3 kPa, 100 fragments/m^2 for 29 kPa, and 1000 fragments/m^2 for 65 kPa. A scaling factor, given in the figure, was used to adjust the densities for glass thicknesses other than 0.3175 cm. This factor indicates that the average maximum density of trapped fragments was 78 percent greater for 0.203-cm glass, and 83 percent less for 0.671-cm glass, than the corresponding density for 0.3175-cm glass.

In some instances, the witness plate was large enough to allow the spatial density of fragments to be measured at angles as large as 22 degrees beyond the edge of the window. Figure 10 shows the ratio of the fragment density to the maximum fragment density plotted as a function of angle beyond the edge of the window. Although there is a large scatter in the data, the regression line indicates that at an angle of 25 degrees the density of glass fragments was approximately one-tenth of the density measured directly behind the window.

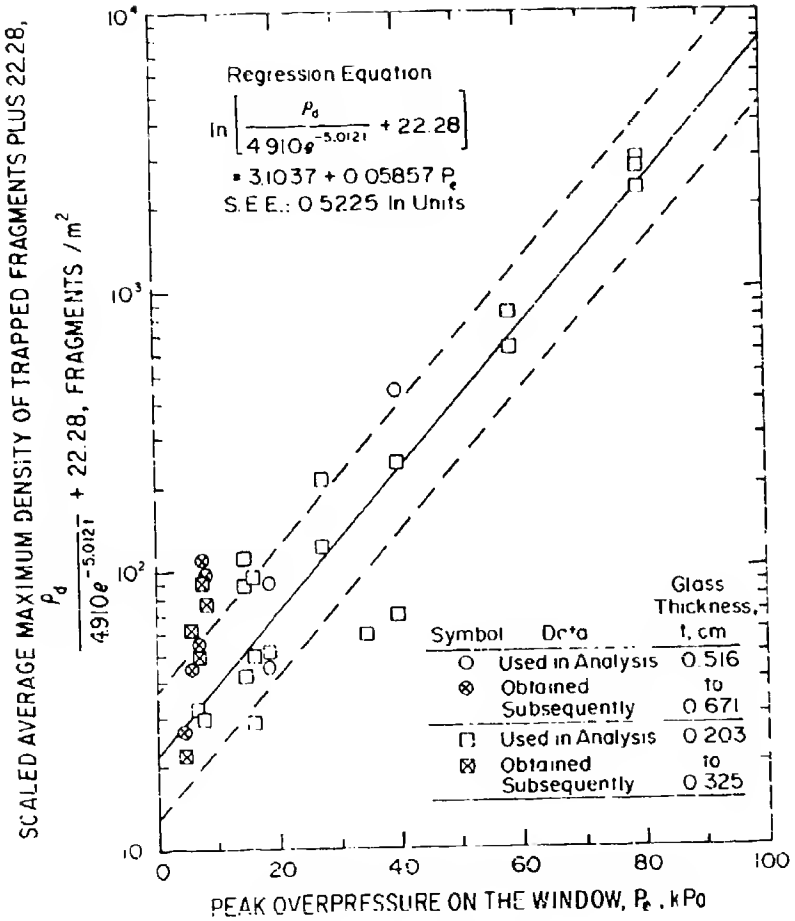

Figure 9. Scaled average maximum density of trapped fragments plus 22.28 vs peak overpressure on the window (after reference 3).

Figure 10. (Average density of fragments trapped at an angle of ψ)/(average maximum density of trapped fragments) vs angle, ψ, beyond the edge of the window.

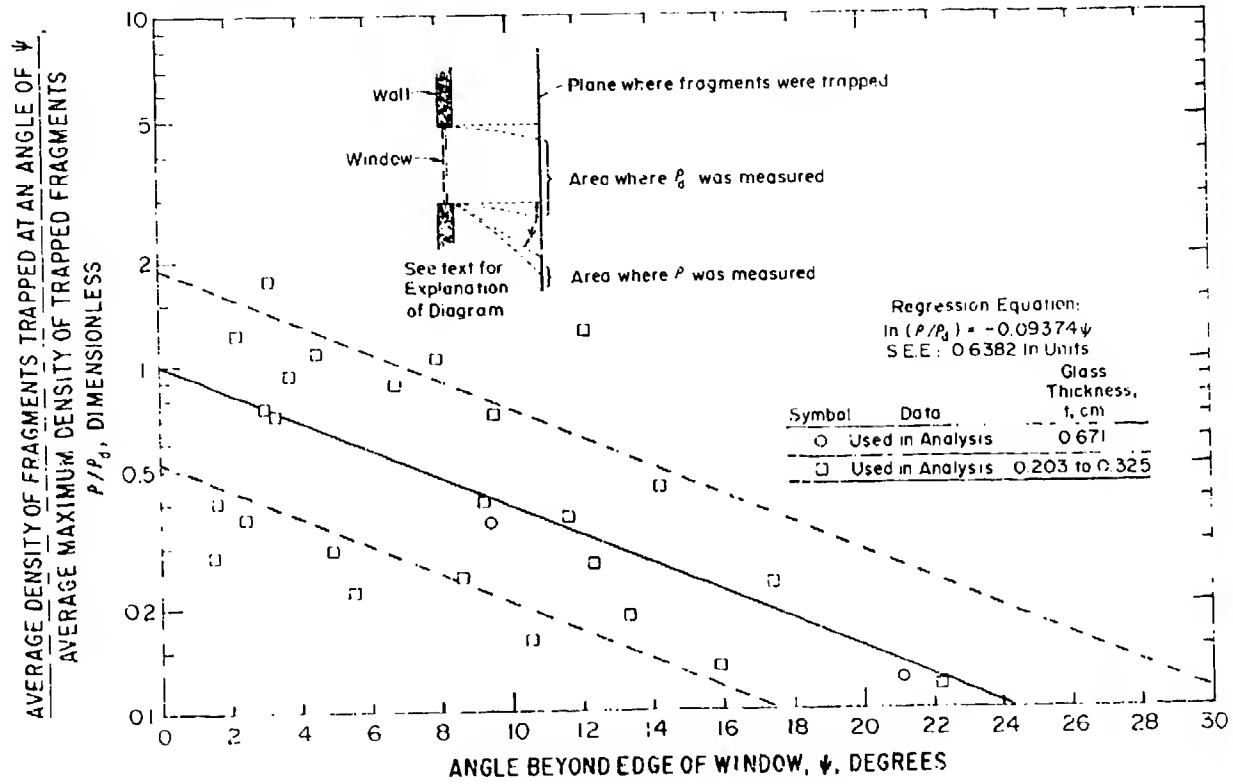

VI. BIOLOGICAL EFFECTS

A. Individual Fragments

Table 2 contains results from experiments in which glass and acrylic fragments were impacted one-at-a-time against anesthesized and sheared sheep and dogs. The small glass fragments (0.0543 to 1.90 gm) with irregular shapes were impacted in a random orientation (Reference 5), whereas the larger glass fragments (1 to 100 gm) with standardized shapes were impacted point on. The acrylic fragments (1 to 100 gm) were irregular in shape but were impacted point-on (cited in Reference 4). The geometric-mean angle subtended by the acrylic fragments is given for each experiment. An angle of 180 degrees indicates that the fragment was square in shape and impacted on one of its edges.

The impact area was either the thorax (between ribs), abdomen, head (in the area of the frontal sinuses), or neck. In some cases, the neck and abdomen were covered with two layers of clothing. The inner layer was an all-cotton tee shirt (145 gm/m^2) and the outer layer was a cotton-sateen material (285 gm/m^2).

The types of injury recorded were (1) skin or body-wall penetration for impacts on the abdomen or thorax and (2) skin penetration or skull fracture (varying from hairline to depressed) for impacts on the head. The average skin thickness was 3 mm for all of the impact areas. The average skin plus body-wall thickness was 18 mm for the thorax and 12 mm for the abdomen. The average skull thickness in the area of the frontal sinuses was 1.3 mm.

Fragments of a given type and mass were impacted at various velocities in order to establish the probability of injury as a function of impact velocity. In each instance it was found that the probability of injury in probit units was approximately linearly related to the logarithm of velocity. A probit analysis was performed on each group of data and the results appear in the last two columns of Table 2. For several groups, there were insufficient data to establish the slope of the probit line, although the fragment velocity for a 50-percent probability of producing the indicated injury was estimated. In the tests using fragments of two thicknesses and a common mass, no significant differences were noted

TABLE 2

FRAGMENT VELOCITIES FOR 50-PERCENT PROBABILITY
OF INDICATED INJURIES TO SHEEP OR DOGS

Fragment Material	Fragment Thickness, cm	Fragment mass, M, gm	Angle Subtended by Fragment, θ, degrees	Exposure Condition of Sheep or Dog*	Impact Area	Injury	$V_{50} \pm E_{V_{50}}$	$b \pm E_b$
Glass	0.312	1	180	Bare	Abdomen or Thorax	Skin penetration Body-wall penetration	55.2 ± 2.1 80.8 ± 3.0	8.81 ± 2.20 14.0 ± 4.6
				Bare	Head	Skin penetration Skull fracture	30.4 ± 2.3 ---#	6.20 ± 3.10 ---
Glass	0.312	1	45	Bare	Abdomen or Thorax	Skin penetration Body-wall penetration	23.6 ± 1.0 42.4 ± 2.1	6.38 ± 2.12 5.39 ± 1.75
				Bare	Head	Skin penetration Skull fracture	21.2 ± 1.5 39.9 ± 3.7	3.56 ± 1.08 ---
Glass	0.312 or 0.569	10	180	Bare	Abdomen or Thorax	Skin penetration Body-wall penetration	39.3 ± 1.2 58.8 ± 1.8	7.08 ± 1.74 7.17 ± 2.19
				Bare	Head	Skin penetration Skull fracture	36.3 ± 1.8 56.3 ± 1.8	9.84 ± 5.19 17.0 ± 6.9
				Clothed	Abdomen	Skin penetration Body-wall penetration	84.1 ± 3.7 99.4 ± 5.2	13.5 ± 5.0 9.03 ± 3.16
Glass	0.312	10	90	Bare	Abdomen or Thorax	Skin penetration Body-wall penetration	20.4 ± 0.9 33.2 ± 1.5	3.65 ± 0.93 4.24 ± 0.87
				Bare	Head	Skin penetration Skull fracture	4.18 ± 0.76 14.7 ± 1.2	--- ---
				Clothed	Abdomen	Skin penetration Body-wall penetration	39.6 ± 2.1 51.5 ± 2.7	4.28 ± 1.73 14.4 ± 4.9
Glass	0.312 or 0.569	10	45	Bare	Abdomen or Thorax	Skin penetration Body-wall penetration	10.2 ± 0.4 15.5 ± 0.7	5.24 ± 1.50 3.72 ± 0.70
				Bare	Head	Skin penetration Skull fracture	3.03 ± 0.66 10.8 ± 0.9	--- 2.81 ± 0.65
				Clothed	Abdomen	Skin penetration Body-wall penetration	13.4 ± 0.7 18.7 ± 1.2	3.91 ± 1.28 11.3 ± 5.4

See footnotes at end of table.

TABLE 2 (Continued)

FRAGMENT VELOCITIES FOR 50-PERCENT PROBABILITY
OF INDICATED INJURIES TO SHEEP OR DOGS

Fragment Material	Fragment Thickness, cm	Fragment mass, M, gm	Angle Subtended by Fragment, θ, degrees	Exposure Condition of Sheep or Dog*	Impact Area	Injury	$V_{50} \pm E_{V50}$	$b \pm E_b$
Glass	0.569	100	180	Bare	Abdomen or Thorax	Skin penetration Body-wall penetration	27.0 ± 1.5 36.0 ± 1.5	3.13 ± 1.56 4.18 ± 1.37
Glass	0.569	100	90	Bare	Abdomen or Thorax	Skin penetration Body-wall penetration	13.0 ± 0.5 18.0 ± 0.8	5.53 ± 1.37 9.83 ± 2.92
				Bare	Head	Skin penetration Skull fracture	1.86 ± 0.34 4.69 ± 0.61	--- ---
Glass	0.569	100	45	Bare	Abdomen or Thorax	Skin penetration Body-wall penetration	5.76 ± 0.79 7.92 ± 0.34	--- 4.30 ± 1.03
				Bare	Head	Skin penetration Skull fracture	1.23 ± 0.23 2.74 ± 0.36	--- ---
Glass	0.25-0.51	0.0543	Random Orientation	Bare	Abdomen	Skin penetration Body-wall penetration	139 ± 12 170 ± 13	--- 2.71 ± 0.73
Glass	0.25-0.51	0.131	Random Orientation	Bare	Abdomen	Skin penetration Body-wall penetration	85.7 ± 5.5 130 ± 8	2.91 ± 0.54 3.28 ± 0.79
Glass	0.25-0.51	0.318	Random Orientation	Bare	Abdomen	Skin penetration Body-wall penetration	62.8 ± 4.1 95.4 ± 5.1	1.96 ± 0.50 1.92 ± 1.01
Glass	0.25-0.51	0.769	Random Orientation	Bare	Abdomen	Skin penetration Body-wall penetration	55.4 ± 4.5 81.1 ± 5.3	2.70 ± 0.82 2.49 ± 0.57
Glass	0.25-0.51	1.90	Random Orientation	Bare	Abdomen	Skin penetration Body-wall penetration	56.9 ± 4.4 65.5 ± 4.9	3.84 ± 1.05 4.72 ± 1.13
Acrylic	0.335	1	48 ± 11	Bare	Abdomen or Thorax	Skin penetration Body-wall penetration	28.0 ± 1.2 67.7 ± 3.0	8.79 ± 2.33 5.95 ± 1.34
Acrylic	0.335	10	64 ± 14	Bare	Abdomen or Thorax	Skin penetration Body-wall penetration	16.2 ± 0.9 32.9 ± 1.2	3.92 ± 0.88 5.45 ± 1.39
				Bare	Head	Skin penetration Skull fracture	7.86 ± 0.85 14.4 ± 2.2	5.90 ± 3.90 6.35 ± 5.29
				Clothed	Abdomen	Skin penetration Body-wall penetration	25.3 ± 1.0 35.4 ± 1.5	11.4 ± 7.6 ---

See footnotes at end of table

TABLE 2 (Continued)

FRAGMENT VELOCITIES FOR 50-PERCENT PROBABILITY
OF INDICATED INJURIES TO SHEEP OR DOGS

Fragment Material	Fragment Thickness, cm	Fragment mass, M, gm	Angle Subtended by Fragment, θ, degrees	Exposure Condition of Sheep or Dog*	Impact Area	Injury	$V_{50} \pm E_{V_{50}}$	$b \pm E_b$
Acrylic	0.335	50	72 ± 9	Bare	Abdomen or Thorax	Skin penetration Body-wall penetration	12.6 ± 0.5 14.8 ± 0.6	6.87 ± 1.67 12.7 ± 3.8
Acrylic	0.335	100	75 ± 18	Bare	Abdomen or Thorax	Skin penetration Body-wall penetration	9.81 ± 0.46 12.3 ± 0.6	5.14 ± 1.33 4.95 ± 1.27
Acrylic	0.335	10	64 ± 14	Bare	Neck	Skin penetration >0.5-cm penetration	15.8 ± 1.2 18.2 ± 2.0	7.23 ± 3.92 4.14 ± 1.21
				Clothed	Neck	Skin penetration >0.5-cm penetration	27.5 ± 1.6 32.9 ± 0.9	6.84 ± 3.53 16.8 ± 8.5

* Dogs were used with glass fragments impacted in a random orientation, and sheep were used in all other cases.

--- Quantity could not be estimated from the data.

The test velocities, which ranged up to 37.2 m/sec, produced no skull fractures.

b Slope of the probit regression line.

V_{50} Fragment velocity for 50% probability of producing the indicated injury, m/sec.

E_b Standard error of b.

$E_{V_{50}}$ Standard error of V_{50}, m/sec.

Notes: The probit regression equation is $Y = 5 + b \ln_e (V/V_{50})$, where V is the fragment velocity in m/sec and Y is the injury probability in probit units.

The acrylic fragments were irregular in shape but impacted point-on. The means and standard deviations of the angles subtended by the fragments are indicated.

Thorax impacts were between ribs, and head impacts were in the area of the frontal sinuses.

in regard to the velocities required to produce a specified injury, and the data were combined. Likewise, no significant differences in injury were noted for impacts on the bare thorax or abdomen, and these data were combined.

Figure 11 is a plot of glass-fragment velocity, V_{50}, for a 50-percent probability of penetrating skin on the thorax or abdomen vs fragment mass, M, and the angle, θ, subtended by the fragment. Figure 12 is the corresponding plot for body-wall penetration. The lines on these figures were computed using the included regression equations derived from the data for glass fragments impacted point on. The equations indicate that, for a given θ and M, the fragment velocity for body-wall penetration is a factor of 1.50 times the corresponding velocity for skin penetration. The lines closely fit the data for point-on impacts, and the lines for a θ of 180 degrees are also a fair approximation to the data for impacts in a random orientation, at least for masses greater than 0.2 gm. For masses below 0.2 gm, the data fall above the lines. Because the regression equations are strictly empirical in nature, it is inadvisable to extrapolate to M's and θ's outside the ranges actually tested.

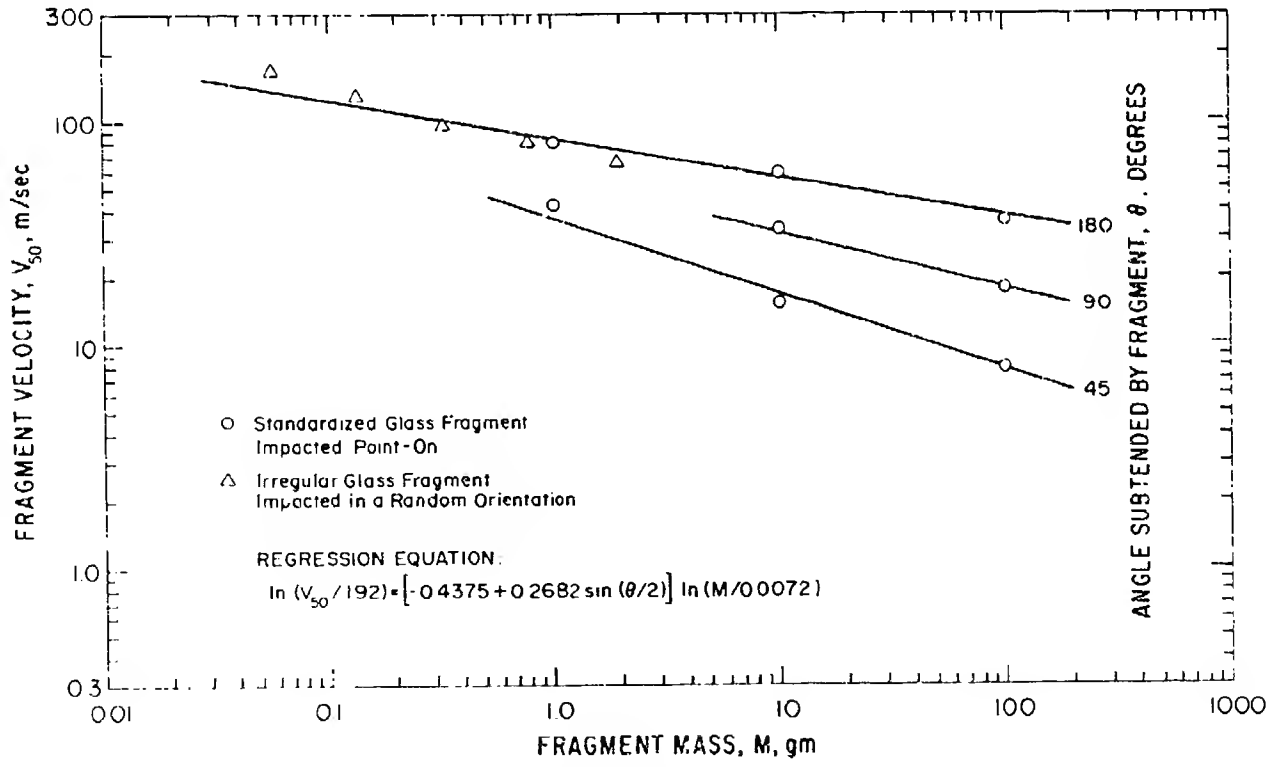

Figure 11. Fifty-percent probability of fragments penetrating skin on the thorax or abdomen.

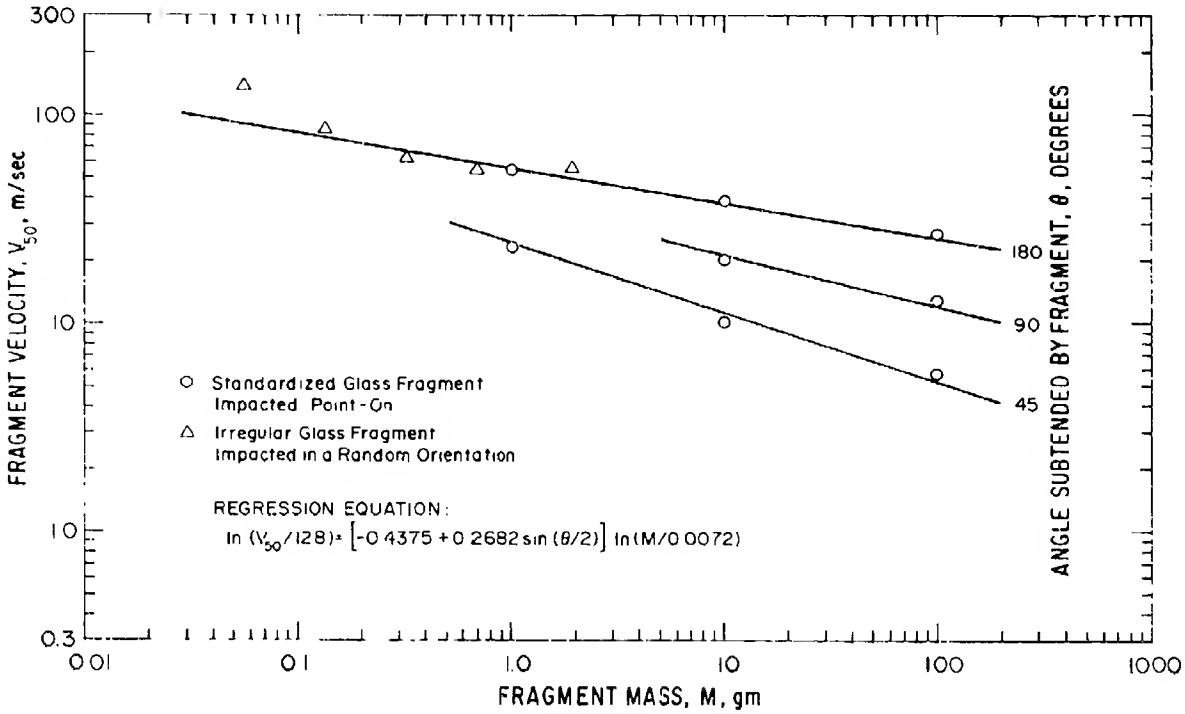

Figure 12. Fifty-percent probability of fragments penetrating body wall of the thorax or abdomen.

Figure 13 shows the relationship between glass-fragment V_{50}, M, and θ for penetrating skin on the head, and Figure 14 shows the corresponding relationship for skull fracture. The curves, which were fitted by eye, indicate that, for a θ of either 45 or 90 degrees, V_{50} decreased with increasing mass. The V_{50} for skin penetration for fragments having a θ of 180 degrees was approximately the same for 1- and 10-gm fragments. Only one datum point was obtained for skull fracture with a θ of 180 degrees.

Figure 15 shows the effect of clothing on the glass- and acrylic-fragment velocities required to penetrate skin or body wall. R_s is the ratio of the V_{50} for skin on the clothed abdomen to the V_{50} for skin on bare thorax or abdomen. R_b is the ratio of the V_{50} for body wall of clothed abdomen to the V_{50} for skin on bare thorax or abdomen. As θ increases above 45 degrees, both ratios appear initially to increase and then to level off at a maximum value of approximately 2.1 for R_s and 2.5 for R_b. Altnough both R_s and R_b

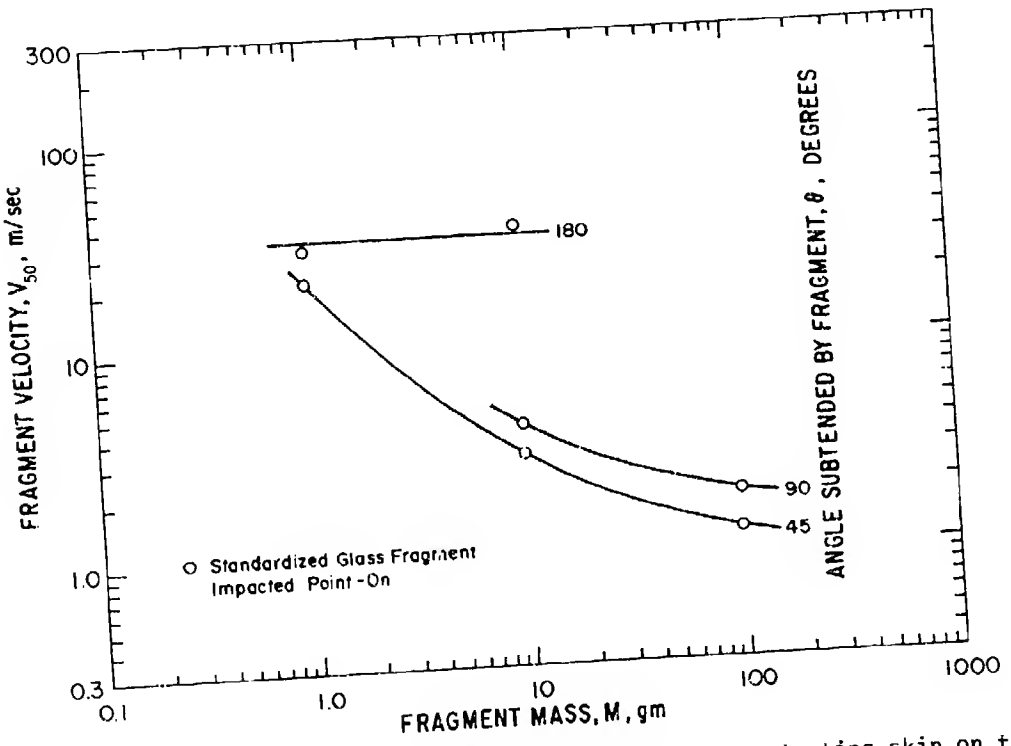

Figure 13. Fifty-percent probability of fragments penetrating skin on the head.

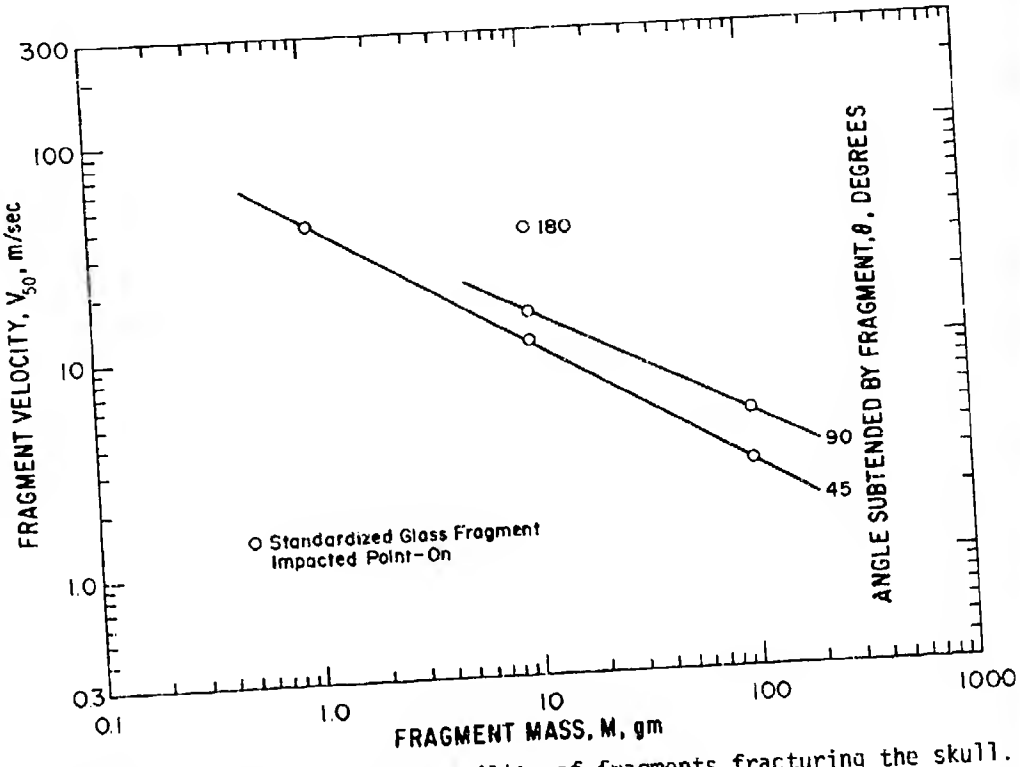

Figure 14. Fifty-percent probability of fragments fracturing the skull.

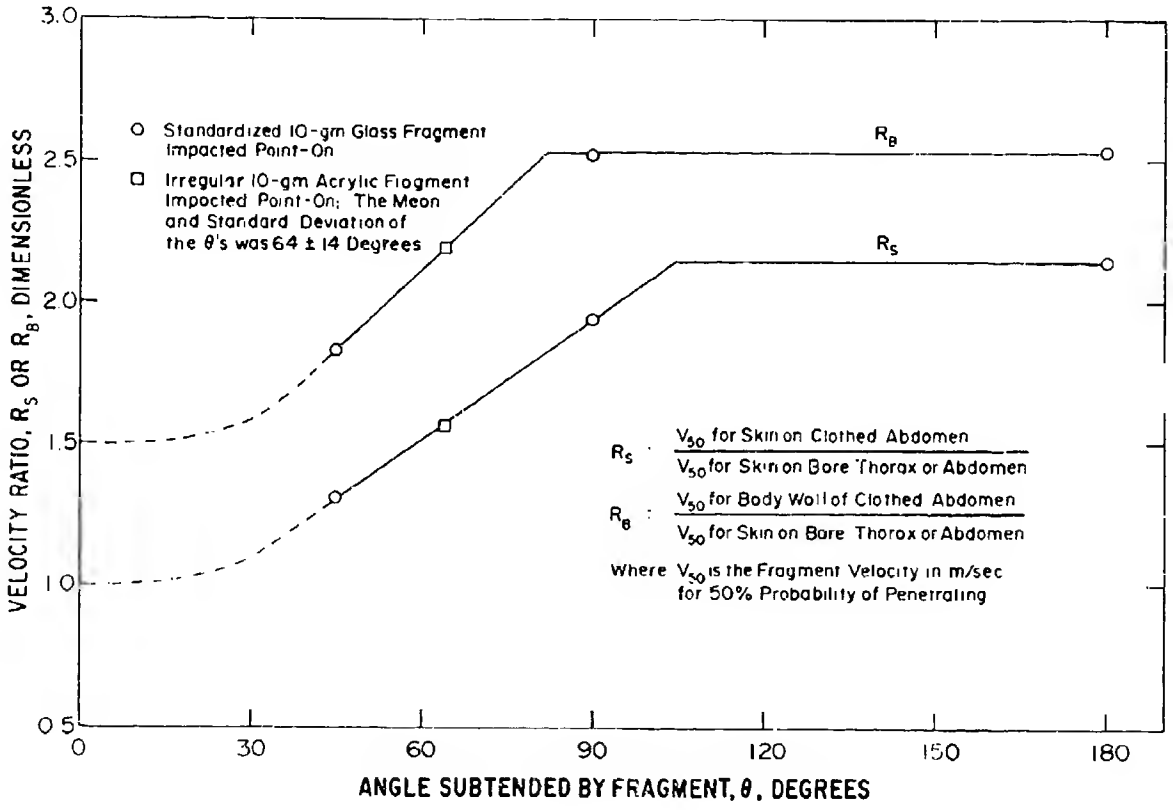

Figure 15. Effects of clothing on fragment velocities required to penetrate skin or body wall.

would be expected to be greater than 1.0 for all values of θ, the R_S curve was extrapolated (dashed portion) to asymptotically approach 1.0 at a θ of zero degrees on the assumption that clothing would offer minimal resistance to a needle-like fragment. It was previously indicated that the ratio of the V_{50} for body wall of bare thorax or abdomen to the V_{50} for skin on bare thorax or abdomen was approximately 1.50 for θ's ranging from 45 to 180 degrees. By assuming that the 1.50 value also applies to a θ of zero degrees, and by again assuming that clothing would offer minimal resistance to needle-like fragments, the R_b curve was extrapolated (dashed portion) to asymptotically approach 1.50 at a θ of zero degrees.

B. Windows

Table 1 gives data for 50 anesthesized and sheared sheep exposed two-at-a-time and side-on either 2.1 or 4.3 m behind a window mounted on the end-plate closing a 3-m-diameter shocktube. Some of the sheep were covered, except for the head, with two layers of clothing similar to that used on the biological tests with individual fragments. The windows were mounted in commercial aluminum frames and complied with standard building codes. Each window consisted of either two 91x91x0.305-cm panes of sheet glass (designated as double-strength) or one 137x183x0.574-cm pane of plate glass.

The panes were broken by blast waves with peak reflected (against the end-plate) overpressures ranging from 4 to 70 kPa and positive-overpressure durations ranging from 46 to 111 msec. Motion-picture records indicated that each biological subject was approximately centered in the pattern of fragments from a window pane. Table 1 lists, for each subject, the maximum wound depth, the total number of incised wounds, and the numbers of skin and body-wall penetrations. The average numbers of the three categories of wounds and the mean impact velocity of the fragments (based upon the averaged impact velocities plotted in Figure 7) were computed for all subjects tested under similar conditions at approximately the same overpressure level. Excluding the data for the one pane that did not break and for the three panes that were 4.3 m from the subjects, these values are plotted in Figure 16. Each of the six sections of the figure shows, for a given type of window and wound, the average number of wounds per bare or clothed subject as a function of the mean impact velocity of the fragments. The curves in Figure 16 are fitted by eye. For each type of wound and window, at all impact velocities, the number of wounds per bare subject was greater than the number per clothed subject, except when both were zero.

At mean impact velocities greater than 40 m/sec, the fragments were so numerous that areas of multiple, closely-clustered, incised wounds of greater than skin depth were observed on all of the bare animals (see Table 1). In these areas there was an increased probability of several fragments' producing contiguous wounds which would have been counted as one wound. This accounts for the fact that, in Figure 16, the bare-subject curves, particularly those for 137x183-cm windows, generally went through a maximum at a velocity of

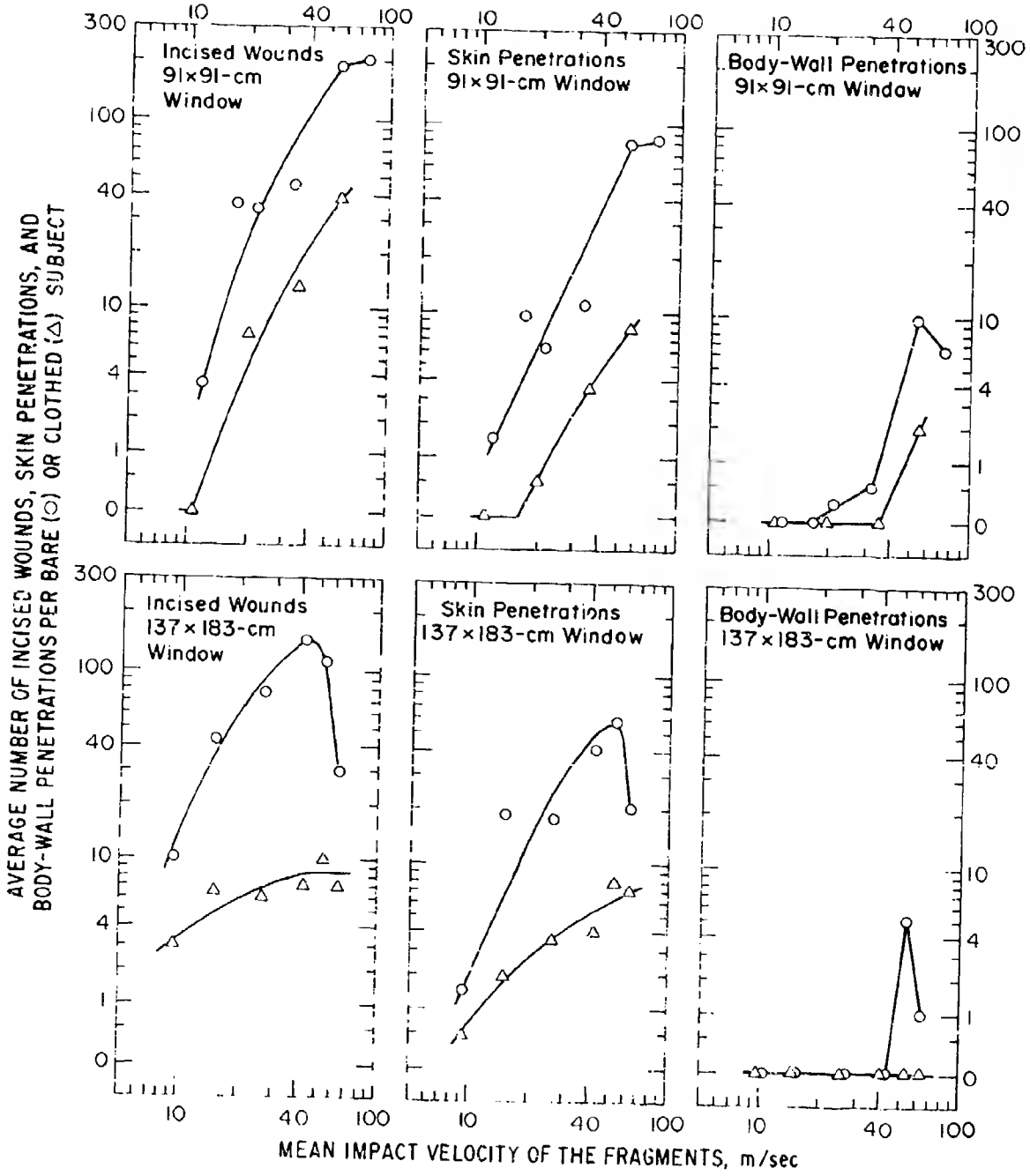

Figure 16. Glass-fragment injuries to subjects behind windows exposed to airblast vs mean impact velocity of the fragments.

approximately 50 m/sec. Although for velocities greater than 50 m/sec the recorded number of wounds decreased, their maximum depths continued to increase with increasing velocity. For mean fragment impact velocities greater than 53 m/sec, all of the bare animals had areas of denudation.

In general, the maximum wound depth increased with increasing fragment impact velocity for clothed subjects as it had for bare subjects. However, areas of multiple, serious, incised wounds or denudation were not observed on any of the clothed subjects. Instead, there were large areas of welting under the clothing at the higher overpressures. The curves for clothed subjects, unlike the curves for bare subjects, do not appear to go through maximums.

The data for subjects 4.3 m from the window are not shown in Figure 16. In general these data suggest that, for similar conditions, the number of injuries of a given type at the 4.3-m range was on the order of one-half of the corresponding number of injuries at the 2.1-m range. The exception to this was for clothed subjects and mean fragment velocities ranging from 41 to 52 m/sec, where the average number of incised wounds was 7 at 2.1 m and 20 at 4.3 m, and the average number of skin penetrations was 4 at 2.1 m and 7 at 4.3 m.

VII. PREDICTION OF WOUNDS VS OVERPRESSURE

The data obtained with sheep behind windows were assumed to apply directly to man. The skin (and body-wall) thickness on a man and a sheep are approximately the same. The surface area exposed to a window would be about 40 percent greater for a face- or back-on man than the corresponding area for a side-on sheep. Therefore, the number of injuries in Table 1 might be low for the extreme case of a man broad-side-on and centered behind a window larger than himself.

In order to use the data obtained with the shocktube to predict the number of wounds for people in houses in relation to blast overpressure, it was necessary to recall that a given overpressure produced larger fragment velocities for windows on the end of the shocktube than for windows in houses. The equation (Figure 6) for the dashed lines in Figure 7

and the measured mean fragment velocity for each window on the shocktube were used to calculate an "effective" peak overpressure which would have produced an equal velocity if the window had been in a house exposed to a long-duration blast wave.

Figure 17 is a plot of the shocktube data (Table 1) for the number of wounds in relation to the calculated "effective" peak overpressure on the window. It should be emphasized that this figure is assumed to apply to people approximately 2 m behind a window in a 1- or 2-story house exposed to a long-duration blast wave. In such cases, the effective peak overpressure would be the actual peak overpressure on the window; i.e., the reflected overpressure for a face-on window and the incident overpressure for a side-on window.

Reference 6 contains experimental data which can be used to confirm the prediction of number of wounds in relation to overpressure. Two unclothed dogs were positioned side-on behind forward-facing windows in two 1-story houses located at the same ground range from a nuclear explosion. The peak incident overpressure was 26 kPa, reflecting to 59 kPa, and the duration of the positive overpressure was 760 msec. The windows consisted of twenty 30x61x 0.32-cm panes of ordinary glass mounted in a steel frame. Each dog was approximately centered 3.4 m behind a window. The measured mean impact velocity of the fragments was 42.7 m/sec. One subject received 36, and the other 37, wounds involving the skin and usually the underlying tissues. One subject received two, and the other six, serious wounds arbitrarily defined as "a laceration penetrating the skin wherein the missile either was stopped by bone or passed into the tissues to a depth of 10 mm or more."

Either Figure 16 and the mean fragment impact velocity of 42.7 m/sec or Figure 17 and the effective peak overpressure of 59 kPa can be used to predict that a sheep located 2.1 m behind a 91x91x0.305-cm window in the same houses would have received approximately 42 skin penetrations and 3 body-wall penetrations. Considering the many variabilities in the experimental arrangements, these numbers are in good agreement with those observed for the two dogs.

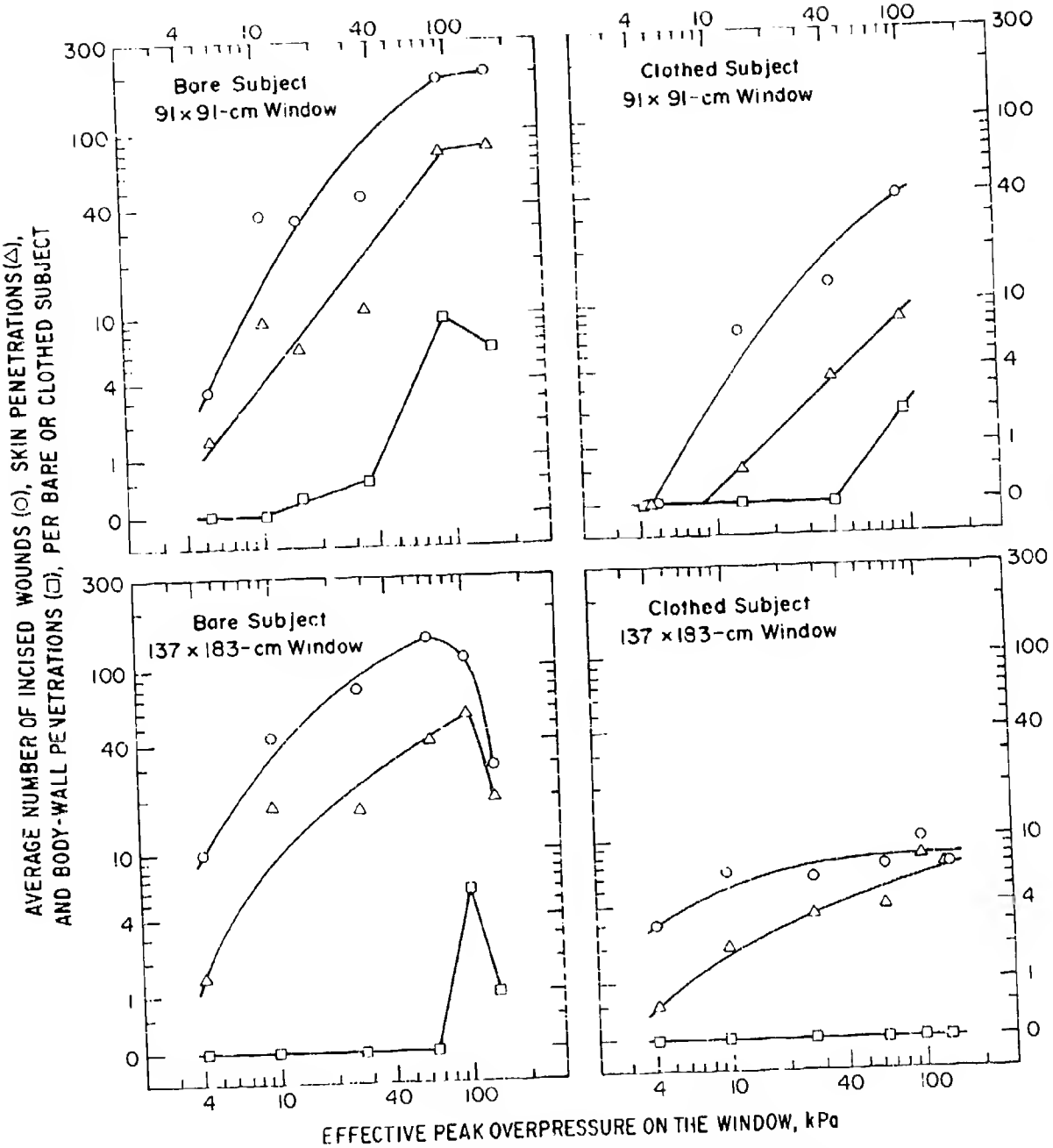

Figure 17. Glass-fragment injuries to subjects behind windows exposed to airblast vs effective peak overpressure on the window.

REFERENCES

1. "The Effects of Nuclear Weapons," (Glasstone, S. and P. J. Dolan, Eds), Third Edition, U. S. Department of Defense and U. S. Department of Energy, Washington, D. C., 1977.

2. Iverson, J. H., "Summary of Existing Structures Evaluation. Part II: Window Glass and Applications," Final Report OCD Work Unit No. 1126C, Stanford Research Institute, Menlo Park, CA, December 1968.

3. Fletcher, E. R., D. R. Richmond and D. W. Richmond, "Airblast Effects on Windows in Buildings and Automobiles on the Eskimo III Event," in Minutes of the Explosives Safety Seminar, 24-26 September 1974, Hollywood, Florida, Volume I, pp. 185-213, Department of Defense Explosives Safety Board, Washington, D. C., September 1974.

4. Fletcher, E. R., "Characteristics and Biological Effects of Fragments from Glass and Acrylic Windows Broken by Airblast," in Proceedings of the DCPA All Effects Research Contractors Conference, 21-25 April 1974, Pacific Grove, California, Research Report 22 Technical Summary, pp. 57-81, Defense Civil Preparedness Agency, Research and Engineering, Washington, D. C., October 1, 1974.

5. Bowen, I. G., D. R. Richmond, M. B. Wetherbe and C. S. White, "Biological Effects of Blast from Bombs. Glass Fragments as Penetrating Missiles and Some of the Biological Implications of Glass Fragmented by Atomic Explosions," USAEC Technical Report, AECU-3350, Office of Technical Services, Department of Commerce, Washington, D. C., June 18, 1956.

6. Goldizen, V. C., D. R. Richmond, T. L. Chiffelle, I. G. Bowen and C. S. White, "Missile Studies with a Biological Target," USAEC Civil Effects Test Group Report, WT-1470, Office of Technical Services, Department of Commerce, Washington, D. C., January 23, 1961.

DISTRIBUTION LIST

DEPARTMENT OF DEFENSE

Armed Forces Radiobiology Rsch Inst
ATTN: Director

Armed Forces Staff College
ATTN: Ref & Tech Svcs Br

Assistant Secretary of Defense
International Security Affairs
ATTN: European & NATO Affairs
ATTN: Policy Plans & NSC Affairs

Assistant Secretary of Defense
Comm, Cmd, Cont & Intell
ATTN: Surv & Warn Sys

Assistant to the Secretary of Defense
Atomic Energy
ATTN: Executive Asst

Command & Control Tech Cen
ATTN: C-312

Defense Intelligence Agency
ATTN: DIA/VPA-2 (Fed Res Div)
ATTN: DB-6
5 cy ATTN: DB-4

Defense Nuclear Agency
ATTN: STNA
ATTN: NATD
ATTN: NATA
ATTN: STSP
ATTN: SPSS
ATTN: RA
6 cy ATTN: TITL

Defense Tech Info Cen
12 cy ATTN: DD

Field Command
Defense Nuclear Agency
ATTN: FCP
ATTN: FC

Field Command
Defense Nuclear Agency
Livermore Branch
ATTN: FCPRL

Interservice Nuclear Weapons Sch
ATTN: TTV

Joint Chiefs of Staff
ATTN: J-3
ATTN: J-5, Strategy Div, W. McClain
ATTN: J-5, Nuclear Div
ATTN: J-3, Strategic Op Div
ATTN: SAGA/SSD
ATTN: SAGA/SFD

National Defense University
ATTN: NWCLB-CR
ATTN: ICAF, Tech Lib

DEPARTMENT OF DEFENSE (Continued)

Joint Strat Tgt Plan Staff
ATTN: JL
ATTN: JLA
ATTN: JP
2 cy ATTN: JLTW-2

Director
NET Assessment
Office of the Secretary of Defense
ATTN: Mil Asst

U.S. National Mil Rep, SHAPE
ATTN: U.S. Doc Off

Under Secretary of Defense for Rsch & Eng.
ATTN: Strategic & Space Sys (OS)
ATTN: Tac War Prog

DEPARTMENT OF THE ARMY

Deputy Chief of Staff for Ops & Plans
Department of the Army
ATTN: DAMO-ZXA
ATTN: DAMO-NC

Harry Diamond Lab., Dept of the Army
ATTN: DELHD-N-P

U.S. Army Ballistic Research Labs
ATTN: DRDAR-TSB-S
ATTN: DRDAR-BLT, Effects Analysis Br

U.S. Army Comd & Gen Staff College
ATTN: ACQ, Lib Div

U.S. Army Concepts Analysis Agency
ATTN: CSSA-ADL

Commander-in-Chief
U.S. Army Europe and Seventh Army
ATTN: AEAGC
ATTN: AEAGE

U.S. Army Nuclear & Chemical Agency
ATTN: Library
ATTN: C. Davidson

U.S. Army TRADOC Sys Analysis Actvy
ATTN: ATAA-TAC

U.S. Army War College
ATTN: Library

U.S. Military Academy, Dept of the Army
ATTN: Doc Lib

DEPARTMENT OF THE NAVY

Naval Postgraduate School
ATTN: Code 1424, Library

Naval Research Lab
ATTN: Code 1240

PRECEDING PAGE BLANK-NOT FILMED

DEPARTMENT OF THE NAVY (Continued)

Naval Sea Systems Command
ATTN: SEA-09G53
ATTN: SEA-643

Naval Surface Weapons Center
ATTN: Code f31

Naval War College
ATTN: Doc Control

Nuclear Weapons Tng Gp, Pacific
Department of the Navy
ATTN: Doc Control

Nuclear Weapons Tng Gp, Atlantic
Department of the Navy
ATTN: Doc Control

Office of Naval Research
ATTN: Tech Info Svcs

DEPARTMENT OF THE AIR FORCE

Air Force School of Aerospace Med
ATTN: Radiobiology Div
ATTN: J. Pickering

Air Force Systems Command
ATTN: DL
ATTN: XR
ATTN: SD

Air Force Weapons Lab
Air Force Systems Command
ATTN: SUL

Air University Lib
Department of the Air Force
ATTN: AUL-LSE

Deputy Chief of Staff
Research, Dev, & Acq
Department of the Air Force
ATTN: AFRDQI

Foreign Technology Div
Air Force Systems Command
ATTN: CCN
ATTN: TQTM
ATTN: SDN

Strategic Air Command
Department of the Air Force
ATTN: NR
ATTN: ADWN
ATTN: XP
ATTN: NRI, STINFO Lib
ATTN: DO

U.S. Air Force, Pacific
ATTN: XP

Commander-in-Chief
U.S. Air Forces in Europe
ATTN: USAFE/DEX

Commander-in-Chief
U.S. Air Forces in Europe
ATTN: USAFE/DOT

DEPARTMENT OF THE AIR FORCE (Continued)

Commander-in-Chief
U.S. Air Forces in Europe
ATTN: USAFE/INA

Commander-in-Chief
U.S. Air Forces in Europe
ATTN: USAFE/INT

Commander-in-Chief
U.S. Air Forces in Europe
ATTN: USAFE/XPX

DEPARTMENT OF ENERGY

Department of Energy
Albuquerque Operations Ofc
ATTN: CTID

Lovelace Biomed & Env Rsch Inst, Inc
4 cy ATTN: D. Richmond
4 cy ATTN: E. Fletcher
4 cy ATTN. J. Yelverton

OTHER GOVERNMENT AGENCIES

Central Intelligence Agency
ATTN: OSWR/NED

Federal Emergency Management Agency
Nat Sec Ofc Mitigation & Rsch
ATTN: Dep Dir, J. Nocita
ATTN: Asst Associated Dir

Department of State
Ofc of International Sec Policy
ATTN: PM/ISP

DEPARTMENT OF ENERGY CONTRACTORS

Lawrence Livermore National Lab
ATTN: Tech Info Dept Lib

Los Alamos National Lab
ATTN: MS 364
ATTN: M/S634, T. Dowler

DEPARTMENT OF DEFENSE CONTRACTORS

Advanced International Studies Inst
ATTN: M. Harvey

Advanced Research & Applications Corp
ATTN: Doc Control

Aerospace Corp
ATTN: Library

BDM Corp
ATTN: J. Braddock

General Electric Co
ATTN: R. Minckler

IIT Research Inst
ATTN: Doc Library

Institute for Defense Analyses
ATTN: J. Grote
ATTN: Class Lib

DEPARTMENT OF DEFENSE CONTRACTORS (Continued)

JAYCOR
ATTN: R. Sullivan

Kaman Sciences Corp
ATTN: F. Shelton

Kaman Sciences Corp
ATTN: E. Daugs

Kaman Tempo
ATTN: DASIAC

Martin Marietta Corp
ATTN: F. Marion

Pacific-Sierra Research Corp
ATTN: G. Lang
ATTN: H. Brode

Pacific-Sierra Research Corp
ATTN: D. Gormely

R & D Associates
ATTN: R. Port
ATTN: P. Haas
2 cy ATTN: Doc Control
2 cy ATTN: S. Borjon

DEPARTMENT OF DEFENSE CONTRACTORS (Continued)

R & D Associates
ATTN: J. Thompson

Science Applications, Inc
ATTN: Doc Control
ATTN: J. Warner
ATTN: M. Drake
ATTN: D. Groce

Science Applications, Inc
ATTN: W. Layson
ATTN: Doc Control

Science Applications, Inc
ATTN: D. Kaul
ATTN: L. Goure

System Planning Corp
ATTN: J. Douglas